OLD DOMINION UNIVERSITY RESEARCH FOUNDATION

SCHOOL OF ENGINEERING
OLD DOMINION UNIVERSITY
NORFOLK, VIRGINIA

Technical Report 75-T9

VISCOUS-SHOCK-LAYER SOLUTIONS FOR TURBULENT FLOW OF RADIATING GAS MIXTURES IN CHEMICAL EQUILIBRIUM

By

E.C. Anderson

and

James N. Moss

Final Technical Report

Prepared for the
National Aeronautics and Space Administration
Langley Research Center
Hampton, Virginia

Under
NASA Grant NSG 1065

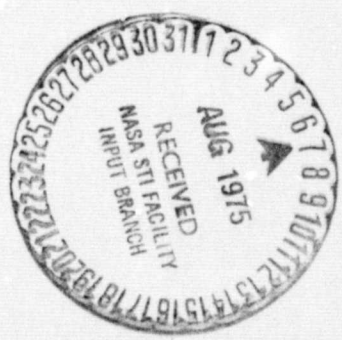

August 1975

VISCOUS-SHOCK-LAYER SOLUTIONS FOR TURBULENT FLOW OF RADIATING GAS MIXTURES IN CHEMICAL EQUILIBRIUM

By

E.C. Anderson[1]

and

James N. Moss[2]

SUMMARY

The viscous-shock-layer equations for hypersonic laminar nad turbulent flows of radiating or nonradiating gas mixtures in chemical equilibrium are presented for two-dimensional and axially-symmetric flow fields. Solutions are obtained using an implicit finite-difference scheme and results are presented for hypersonic flow over spherically-blunted cone configurations at freestream conditions representative of entry into the atmosphere of Venus. These data are compared with solutions obtained using other methods of analysis.

---

[1] Research Associate, School of Engineering, Old Dominion University, Norfolk, Virginia 23508.

[2] National Aeronautics and Space Administration - Langley Research Center, Hampton, Virginia 23665.

SYMBOLS

A^+ damping factor [eqs. (15) and (16)]

C_i mass fraction of species i, ρ_i/ρ

C_ℓ mass fraction of element ℓ

C_p frozen specific heat of mixture, $\sum_{i=1}^{N} C_i C_{p,i}$

$C_{p,i}$ specific heat of species i, $C^*_{p,i}/C^*_{p,\infty}$

H defined quantity, $h + \frac{u^2}{2}$

H_t total enthalpy, $H + \frac{v^2}{2}$

h enthalpy of mixture, $\sum_{i=1}^{N} C_i h_i$

h_A enthalpy of undecomposed ablation material

h_i enthalpy of species i, h^*_i/U^{*2}_∞

j flow index: 0 for plane flow; 1 for axisymmetric flow

K thermal conductivity of mixture, $K^*/\mu^*_{ref} C^*_{p,\infty}$

ℓ mixing length [eq. (13)]

M^* molecular weight

$\bar{M}^*$ molecular weight of mixture

N number of species

N_{Le} Lewis number, $\rho^* D^*_{ij} C^*_p / K^*$

$N_{Le,T}$ turbulent Lewis number

N_{Pr} Prandtl number, $\mu^* C_p^*/K^*$

$N_{Pr,T}$ turbulent Prandtl number, $\mu_T^* C_p^*/K_T^*$

N_{Re} Reynolds number, $\rho_\infty^* U_\infty^* r_n^*/\mu_\infty^*$

N_{Sc} Schmidt number, $N_{Sc} = N_{Pr}/N_{Le}$

n coordinate measured normal to body, n^*/r_n^*

n^+ normal coordinate [eq. (22)]

P^+ pressure-gradient parameter [eq. (25)]

p pressure, $p^* \Big/ \left[\rho_\infty^* \left(U_\infty^*\right)^2\right]$

Q divergence of the net radiant heat flux, $Q^* R_N^*/\rho_\infty^* U_\infty^{*3}$

q_r net radiant heat flux in n-direction, $q_r^*/\rho_\infty^* U_\infty^{*2}$

$q_r^{(+)*}$ component of radiant flux toward the shock

$q_r^{(-)*}$ component of radiant flux toward the wall

$-q_{c,w}$ convective heat flux to the wall [eq. (13)]

r radius measured from axis of symmetry to point on body surface, r^*/r_n^*

r_n^* nose radius

s coordinate measured along body surface, s^*/r_n^*

T temperature, T^*/T_{ref}^*

T^*_{ref}	temperature, $(U^*_\infty)^2/C^*_{p,\infty}$
U^*_∞	free-stream velocity
u	velocity component tangent to body surface, u^*/U^*_∞
u_t	friction velocity [eq. (19)]
v	velocity component normal to body surface, v^*/U^*_∞
v^+	scaled mean velocity component [eq. (18)], v_w/u_t
α	shock angle defined in figure 1
β	angle defined in figure 1
$\gamma_{i,\eta}$	normal intermittency factor [eq. (30)]
δ	boundary-layer thickness
δ_k	incompressible displacement thickness [eq. (29)]
$\delta_{i\ell}$	number of atoms of the ℓth element in species i
ε^+	normalized eddy viscosity, μ_T/μ
ε^+_i	eddy viscosity, inner law [eq. (12)]
ε^+_o	eddy viscosity, outer law [eq. (20)]
η	transformed n-coordinate, n/n_s
θ	body angle defined in figure 1
κ	body curvature

μ molecular viscosity, $\mu^*/\mu^*(T^*_{ref})$

μ_T eddy viscosity

ξ coordinate measured along body surface, $\xi = s$

ρ density of mixture, ρ^*/ρ^*_∞

σ Reynolds number parameter, $\left[\frac{\mu^*\ (T^*_{ref})}{\rho^*_\infty U^*_\infty r^*_n}\right]^{1/2}$

σ^* Stefan-Boltzmann constant

$\phi_{1,2,3}$ quantities defined by equations (4b, 4c, 4d)

Superscripts:

j 0 for plane flow; 1 for axisymmetric flow

- quantity divided by its corresponding shock value

* dimensional quantity

' total differential or fluctuating component

" shock-oriented velocity component (see fig. 1)

Subscripts:

e boundary-layer edge

i ith species

ℓ ℓth element

s	shock
w	wall
∞	free stream
-	values for the solid ablation material at the surface

INTRODUCTION

Numerical methods for calculating flow fields with ablation products injected into a radiating gas mixture in chemical equilibrium have been developed by Sutton (ref. 1) and Moss (ref. 2) for the analysis of hypersonic flow over blunt entry probe configurations. The numerical solution procedure developed by Sutton is applicable to laminar, transitional, and turbulent flow and is obtained using a coupled inviscid flow-boundary-layer analysis. The inviscid flow solution is determined by an explicit time dependent finite-difference scheme similar to the method developed by Barnwell (ref. 3), and the boundary-layer equations are solved by use of an integral matrix procedure (BLIMP) developed by Bartlett and Kendall (ref. 4).

Moss' analysis is restricted to laminar flow and solutions are determined using an implicit finite-difference scheme developed by Davis (ref. 5) for solving the viscous-shock-layer equations. The principal advantages of this technique are that the solution is direct and that the effects of inviscid-viscous interactions are included within a single set of governing equations which are uniformly valid throughout the shock layer.

In the analyses presented by Sutton and Moss, the radiation heat transfer is calculated using the method developed by Nicolet (refs. 6 and 7). This radiation model assumes a nongray gas and accounts for molecular band, atomic line, and continuum transitions.

The present report presents the development of a viscous-shock-layer analysis applicable to laminar and turbulent flow of radiating

or nonradiating gas mixtures in chemical equilibrium. This analysis is based upon the viscous-shock-layer analysis applicable to turbulent flow of perfect gases developed by Anderson and Moss (ref. 8) and the laminar viscous-shock-layer analysis for equilibrium chemistry developed by Moss (ref. 2).

Results obtained with the present method of analysis are compared with methods which include corrections for inviscid-viscous interactions. Solutions are presented for a 120-degree (total angle) spherically-blunted cone configuration at freestream conditions representative of entry into the atmosphere of Venus. Heating-rate distributions are compared for a cold wall (freestream temperature) nonradiating shock layer and a radiating shock layer with injected ablation products.

The availability of comparative data obtained using methods corrected for inviscid-viscous interactions is limited. Consequently, the data obtained using the present method of analysis are to be considered as preliminary and serve primarily to establish stability of the numerical method. It is emphasized that no attempts have been made to obtain better agreement with either of the analyses used in the comparisons. A more extensive data base is necessary to establish the validity of the present solution procedure.

ANALYSIS

Governing Equations

The equations of motion for reacting gas mixtures in chemical equilibrium are presented by Bird, Stewart, and Lightfoot (ref. 9). The formulation of these equations in body-oriented coordinates appropriate for viscous-shock-layer analysis of laminar flow of radiating and nonradiating gases is presented by Moss (ref. 2).

For turbulent flow, the viscous-shock-layer equations are derived using methods analogous to those presented by Dorrance (ref. 10) for the turbulent-boundary-layer equations and are expressed in non-dimensional form for the coordinate system shown in figure 1 as:

Continuity:

$$\frac{\partial}{\partial s}\left[(r + n\cos\theta)^j \rho u\right] + \frac{\partial}{\partial n}\left[(1 + n\kappa)(r + n\cos\theta)^j \rho v\right] = 0 \qquad (1)$$

s-momentum:

$$\rho\left(\frac{u}{1 + n\kappa}\frac{\partial u}{\partial s} + v\frac{\partial u}{\partial n} + \frac{uv\kappa}{1 + n\kappa}\right) + \frac{1}{1 + n\kappa}\frac{\partial p}{\partial s} = \sigma^2\left\{\frac{\partial}{\partial n}\left[\mu(1 + \varepsilon^+)\left(\frac{\partial u}{\partial n} - \frac{u\kappa}{1 + n\kappa}\right)\right] + \left(\frac{2\kappa}{1 + n\kappa} + \frac{j\cos\theta}{r + n\cos\theta}\right)\left[\mu(1 + \varepsilon^+)\left(\frac{\partial u}{\partial n} - \frac{u\kappa}{1 + n\kappa}\right)\right]\right\} \qquad (2)$$

n-momentum:

$$\rho\left(\frac{u}{1 + n\kappa}\frac{\partial v}{\partial s} + v\frac{\partial v}{\partial n} - \frac{u^2\kappa}{1 + n\kappa}\right) + \frac{\partial p}{\partial n} = 0 \qquad (3)$$

Energy:

$$\rho\left(\frac{u}{1 + n\kappa}\frac{\partial H}{\partial s} + v\frac{\partial H}{\partial n}\right) - v\frac{\partial p}{\partial n} + \frac{\rho u^2 v\kappa}{1 + n\kappa} = \sigma^2\left[\frac{\partial}{\partial n}(\phi_1 + \phi_2 + \phi_3) + \left(\frac{\kappa}{1 + n\kappa} + \frac{j\cos\theta}{r + n\cos\theta}\right)(\phi_1 + \phi_2 + \phi_3)\right] - Q \qquad (4a)$$

where

$$\phi_1 = \frac{\mu}{N_{Pr}}\left(1 + \varepsilon^+\frac{N_{Pr}}{N_{Pr,T}}\right)\frac{\partial H}{\partial n} \qquad (4b)$$

$$\phi_2 = \frac{\mu}{N_{Pr}} \left[N_{Pr} - 1 + \frac{\varepsilon^+ N_{Pr}}{N_{Pr,T}} \left(N_{Pr,T} - 1 \right) \right] u \frac{\partial u}{\partial n} - \mu(1 + \varepsilon^+) \frac{u^2 \kappa}{1 + n\kappa} \quad (4c)$$

$$\phi_3 = \frac{\mu}{N_{Pr}} \left[N_{Le} - 1 + \varepsilon^+ \frac{N_{Pr}}{N_{Pr,T}} \left(N_{Le,T} - 1 \right) \right] \sum_{i=1}^{N} h_i \frac{\partial C_i}{\partial n} \quad (4d)$$

and

$$H \equiv h + \frac{u^2}{2} \quad (4e)$$

Elemental continuity:

$$\rho \left(\frac{u}{1 + n\kappa} \frac{\partial \tilde{C}_l}{\partial s} + v \frac{\partial \tilde{C}_l}{\partial n} \right) = \frac{\sigma^2}{(1 + n\kappa)(r + n \cos \theta) j} \times \quad (5a)$$

$$\frac{\partial}{\partial n} \left\{ \left[(1 + n\kappa)(r + n \cos \theta)^j \frac{\mu}{N_{Pr}} \left(N_{Le} + \varepsilon^+ \frac{N_{Pr}}{N_{Pr,T}} N_{Le,T} \right) \frac{\partial \tilde{C}_l}{\partial n} \right] \right\}$$

where

$$\tilde{C}_l = \sum_{i=1}^{N} \delta_{i_l} \frac{M^*_l}{M^*_i} C_i \quad (5b)$$

State:

$$p = \rho T R^* / \bar{M}^* C^*_{p,\infty} \quad (6)$$

Boundary conditions. The boundary conditions at the shock are calculated by using the Rankine-Hugoniot relations. At the wall, the no-slip and no-temperature-jump boundary conditions are used; consequently, $u_w = 0$. The wall temperature and mass injection rate are either specified or calculated. For the calculated mass injection conditions, the ablation process is assumed to be quasi-steady and the wall temperature is the sublimation temperature of the ablator surface. With these assumptions, the expression for the coupled mass injection rate is

$$\dot{m} = \left(\frac{-q^*_{c,w} - q^*_{r,w}}{\sum_{i=1}^{N} (C_i h^*_i)_w - h^*_A} \right) \left(\frac{1}{\rho^*_\infty U^*_\infty} \right) \tag{7}$$

For ablation injection, the elemental concentrations at the wall are governed by convection and diffusion as given by the equation

$$\left(\frac{\partial \tilde{C}_\ell}{\partial n} \right)_w - \frac{1}{\sigma^2} \left(\frac{\dot{m} N_{Sc}}{\mu} \right)_w \left[\left(\tilde{C}_\ell \right)_w - \left(\tilde{C}_\ell \right)_- \right] = 0 \tag{8}$$

Precursor effects are neglected while the energy reradiated from the surface is included in the radiation transport calculations. The net radiative flux, q_r, can be represented as the difference of two components

$$q_r = q_r^{(+)} - q_r^{(-)} \tag{9}$$

At the surface

$$q_{r,w}^{(+)*} = \varepsilon \sigma^* T_w^{*4} \tag{10}$$

where ε is the emissivity of the ablator.

The heat transferred to the wall due to conduction and diffusion is

$$-q_{c,w} = \sigma^2 \left(K \frac{\partial T}{\partial n} + \frac{\mu}{N_{Sc}} \sum_{i=1}^{N} h_i \frac{\partial C_i}{\partial n} \right)_w \tag{11}$$

Radiative transport. The radiative flux, q_r, and the divergence of the radiative flux, Q, are calculated with the radiative transport code RAD, as presented in references 6 and 7. The RAD computer code has been incorporated in the present viscous-shock-layer computer code (HYVIS) and streamlined for computational efficiency.

The RAD code accounts for the effects of nongray self-absorption and radiative cooling. Molecular band, continuum, and atomic line transitions are included. A detailed frequency dependence of the absorption coefficients is used for integrating over the radiation frequency spectrum and the tangent slab approximation is used for integrating over physical space.

Thermodynamic and transport properties. The equilibrium composition is determined by a free energy minimization calculation as developed in reference 11. Thermodynamic properties for specific heat, enthalpy, and free energy and transport properties for viscosity and thermal conductivity are required for each species considered. Values for the thermodynamic (refs. 12 and 13) and transport properties (ref. 14) are obtained by using polynomial curve fits. The mixture viscosity is obtained by using the semi-empirical formulae of Wilke (ref. 15).

Eddy-Viscosity Approximations

A two-layer eddy-viscosity model consisting of an inner law based upon Prandtl's mixing-length concept and the Clauser-Klebanoff expression (based on refs. 16 and 17) for the outer law is used in the present investigation. This model, introduced by Cebeci (ref. 18),

assumes that the inner law is applicable for the flow from the wall outward to the location where the eddy viscosity given by the inner law is equal to that of the outer law. The outer law is then assumed applicable for the remainder of the viscous layer. It is noted that the eddy viscosity degenerates to approximately zero in the inviscid portion of the shock layer. The degeneracy is expressed in terms of the normal intermittency factor given by Klebanoff (ref. 17). The expressions used in the present investigation are given in the following sections.

Inner-eddy-viscosity approximation. Prandtl's mixing-length concept is stated in non-dimensional variables as

$$\epsilon_i^+ = \frac{\rho \ell^2}{\sigma^2 \mu} \left| \frac{\partial u}{\partial n} \right| \tag{12}$$

The mixing length ℓ is evaluated by using Van Driest's proposal (ref. 19) stated as

$$\ell = k_1 n \left[1 - \exp\left(- \frac{n^+}{A^+} \right) \right] \tag{13}$$

where

$$n^+ = \frac{n\rho}{\sigma^2 \mu} \left[\frac{\mu_w}{\rho} \left(\frac{\partial u}{\partial n} \right) \right]_w^{1/2} \tag{14}$$

Here, k_1 is the Von Kármán constant, which is assumed to have a value of 0.4, and A^+ is a damping factor.

Cebeci (ref. 18) suggests that for flows with a pressure gradient, the damping factor be expressed as

$$A^+ = 26(1 - 11.8P^+)^{-1/2} \tag{15}$$

and for flows with both a pressure gradient and mass injection,

$$A^+ = 26 \left\{ - \frac{P^+}{v^+} \left[\exp\,(11.8v^+) - 1 \right] + \exp\,(11.8v^+) \right\}^{-1/2} \tag{16}$$

where

$$p^+ = -\sigma^2 \left(\frac{\partial p}{\partial s}\right)_e \frac{\mu}{\rho^2 u_\tau^3} \tag{17}$$

$$v^+ = \frac{v_w}{u_\tau} \tag{18}$$

and

$$u_\tau = \sigma \left[\frac{\mu_w}{\rho} \left(\frac{\partial u}{\partial n}\right)_w\right]^{1/2} \tag{19}$$

Outer-eddy-viscosity approximation. For the outer region of the viscous layer the eddy viscosity is approximated by the Clauser-Klebanoff expression

$$\varepsilon_o^+ = \frac{k_2 \rho u_e \delta_k \gamma_{i,\eta}}{\sigma^2 \mu} \tag{20}$$

where

$$\delta_k = \int_0^\delta \left(1 - \frac{u}{u_e}\right) dn$$

$$k_2 = 0.016 \tag{21}$$

and

$$\gamma_{i,\eta} = \left[1 + 5.5 \left(\frac{n}{\delta}\right)^6\right]^{-1} \tag{22}$$

Equation (22) is Cebeci's approximation (ref. 18) of the error-function definition presented by Klebanoff (ref. 17).

For equilibrium flow without radiation, the boundary-layer thickness δ is assumed to be the value of n at the point where

$$\frac{H_t}{H_{t,\infty}} = 0.995 \tag{23}$$

and is defined by linear interpolation in an array of local total enthalpies. This definition is approximately equivalent to the usual boundary-layer definition

$$\frac{u}{u_e} = 0.995 \tag{24}$$

where u_e is the local value for the undisturbed inviscid flow outside the boundary layer.

The values of the parameters k_1 and k_2 in equations (13) and (20) depend on the flow conditions being considered, as does the constant represented by the value 26 in equations (15) and (16). The values given are used for convenience in developing the numerical method.

For radiating gases, the loss of energy from the shock layer makes the total enthalpy definition unsatisfactory. For these cases, the boundary-layer thickness is assumed to be that portion of the shock layer which contributes 95% of the dissipated energy, and is defined by the expression

$$\frac{\int_0^{\delta} \frac{\tau^2}{\mu(1+\varepsilon^+)}\,dn}{\int_0^{N_s} \frac{\tau^2}{\mu(1+\varepsilon^+)}\,dn} = 0.95 \tag{25}$$

This definition shows acceptable agreement with the total enthalpy definition when applied to nonradiating flows and should be an acceptable definition for radiating gases.

Method of Solution

Davis (ref. 5) presented a method for solving the viscous-shock-layer equations for stagnation and downstream flow. Moss (ref. 2) applied this method of solution to reacting multicomponent mixtures. The present method of solution is identical to that of references 2 and 5. Therefore, only an overview of the solution procedure is presented here.

The numerical computation is simplified by normalizing most of the variables with their local shock values. The transformed independent and dependent variables are

$$\left.\begin{aligned} \eta &= n/n_s & \bar{p} &= p/p_s \\ \xi &= s & \bar{\rho} &= \rho/\rho_s \\ \bar{u} &= u/u_s & \bar{T} &= T/T_s \\ \bar{v} &= v/v_s & \bar{H} &= H/H_s \\ \bar{\mu} &= \mu/\mu_s & \bar{K} &= K/K_s \end{aligned}\right\} \tag{26}$$

Since the normal coordinate, n, is normalized with respect to the local shock stand-off distance, a constant number of finite-difference grid points between the body and shock are used. The transformations relating the differential quantities are

$$\frac{\partial}{\partial s} = \frac{\partial}{\partial \xi} - \frac{n_s'}{n_s}\,\eta\,\frac{\partial}{\partial \eta} \tag{27a}$$

where

$$n_s' = \frac{dn_s}{d\xi} \tag{27b}$$

$$\frac{\partial}{\partial n} = \frac{1}{n_s}\,\frac{\partial}{\partial \eta} \tag{27c}$$

and

$$\frac{\partial^2}{\partial n^2} = \frac{1}{n_s^2} \frac{\partial^2}{\partial \eta^2} \tag{27d}$$

The three second-order partial differential equations are linearized and written in the standard form for a parabolic equation as

$$\frac{\partial^2 W}{\partial \eta^2} + \alpha_1 \frac{\partial W}{\partial \eta} + \alpha_2 W + \alpha_3 + \alpha_4 \frac{\partial W}{\partial \xi} = 0 \tag{28}$$

where W represents tangential velocity for the s-momentum equation, enthalpy for the energy equation, and elemental concentrations for the elemental continuity equations. For the energy equation, the divergence of the radiative flux is incorporated in the α_3 term. When the derivatives in equation (28) are converted to finite-difference form by using Taylor's series expansions, the resulting equations are of the following form:

$$A_n W_{m,n-1} + B_n W_{m,n} + C_n W_{m,n+1} = D_n \tag{29}$$

The subscript n denotes the grid points along a line normal to the body surface, and the subscript m denotes the grid stations along the body surface. Equation (29), along with the boundary conditions, constitute a system of the tridiagonal form and can be solved efficiently.

A variable grid spacing is used in both the tangential and normal directions to the surface so that the grid spacing can be made small in the region of large gradients. The order of the truncation terms neglected are $\Delta\xi$ (first order accurate) and either $\Delta\eta_n \Delta\eta_{n-1}$ or $(\Delta\eta_n - \Delta\eta_{n-1})$.

The equations are solved at any body station m in the order shown in figure 2. The governing equations are uncoupled and the values of the dependent variables are computed one at a

time. Each of the second-order differential equations is individually integrated numerically by using the tridiagonal formalism [eq. (29)]. The global continuity equation is used to obtain both shock stand-off distance and the $\bar{v}$ components of velocity. By integrating the global continuity equation between the limits of 0 to 1, a quadratic equation for n_s is obtained. For the $\bar{v}$ component of velocity at η, the global continuity equation is integrated with respect to η between the limits of 0 to η. The pressure, p, is determined at station m by integrating the normal momentum equation with respect to η between the limits of 1 to η. The equation of state is used to determine the density. The solution is iterated until convergence is achieved. The solution advances to the next body station, m + 1, and uses the previous converged solution profiles as initial values for starting the solution at station m + 1. This procedure is repeated until a solution pass is obtained.

The first solution pass provides a first approximation to the flow field solution because the following assumptions are used. The thin shock-layer form of the n-momentum equation, $\frac{\rho u^2 \kappa}{1 + n\kappa}$, is used; the stagnation streamline solution is independent of downstream influence; the term $dn_s/d\xi$ is set to zero at each body station; and the shock angle α is assumed to be the same as the body angle θ. These approximations are then removed by global iteration. Two solution passes are generally sufficient. This solution procedure is programmed for the CDC 6600 computer.

DISCUSSION AND RESULTS

Numerical solutions obtained with the present method of analysis are compared with an integral boundary-layer solution for a non-radiating shock layer with a cold wall boundary condition, and with a solution which couples the inviscid flow and boundary-layer equations for a radiating shock layer with surface ablation.

For the nonradiating shock layer with a cold wall boundary condition, solutions were determined by Edquist* using the integral

* The boundary-layer data have not been published and are presented by permission of C.T. Edquist, Martin Marietta Corp., Denver Division, Denver, CO.

boundary-layer solution procedure (SHIV) discussed in reference 20. Freestream conditions correspond to a typical trajectory point for entry into the atmosphere of Venus. The freestream velocity, temperature, and density are 10 km/s, 200 K, and 0.01 kg/m^3, respectively. The atmospheric composition expressed in mole fractions is 0.95 CO_2 and 0.05 N_2. The body considered is a 120-degree (total angle) spherically-blunted cone having a nose radius of 0.368 m and a base radius of 0.66 m. The surface temperature is assumed to be equal to that of the freestream.

The inviscid flow field solution used to specify edge conditions for the boundary-layer solutions was determined using a single strip integral method which accounts for the upstream influence of the sonic corner. This influence cannot be accounted for in the present analysis, but as shown in figure 3, this influence is significant only in the region $1.6 \leq r/r_n \leq 2$. For $r/r_n < 1.6$, the maximum difference in the surface-pressure distribution computed using the present method and the single strip integrated method is less than 4%.

Heat-transfer rate distributions corresponding to boundary-layer solutions for isentropic expansion edge conditions (and for edge conditions corrected for vorticity effects) are compared with the present method of solution in figure 4. It is noted that the present analysis was obtained assuming instantaneous transition from laminar to turbulent flow. The heat-transfer rate correlation formula used in the boundary-layer analysis includes a transition correction. Both the present analysis and the boundary-layer analysis corrected for vorticity effects show a significant increase in heat transfer when compared with the boundary-layer solution for isentropic expansion edge conditions. The present analysis and the corrected boundary-layer analysis differ by as much as 30% in the region of fully developed turbulent flow. Considering the assumption of local similarity used in the integral boundary-layer analysis and the different methods of turbulence modeling, the differences between the two methods of solution is not excessive.

The solution presented for a radiating shock layer with injection of ablation products corresponds to the Venus entry conditions used in the coupled inviscid flow-boundary-layer analysis presented by Sutton (ref. 1). The atmospheric composition expressed in mole fractions is assumed to be 0.97 CO_2 and 0.03 N_2. Freestream velocity, temperature, and density are 8.8 km/s, 180 K, and 0.0058 kg/m^3, respectively. The geometry considered is a 120-degree (total angle) spherically-blunted cone having a nose radius of 0.325 m and a base radius of 0.69 m. The ablator material is carbon-phenolic having a composition expressed in mass fractions of 0.11 O, 0.004 N, 0.851 C, and 0.035 H.

The surface ablation-rate distribution used in the present analysis corresponds to that determined by Sutton (ref. 1), and is shown in figure 5. Comparisons of the surface-pressure distributions and shock shapes corresponding to the present analysis and that of reference 1 are shown in figures 6 and 7, respectively. The maximum differences in the surface-pressure distributions and shock-layer thicknesses determined by the two methods of analysis are approximately 3%. Since the inviscid solution does not account for displacement effects, the differences noted are expected for the specified injection rates. Other properties within the essentially inviscid portion of the shock layer show similar agreement.

Comparisons of radiative and convective heating-rate distributions corresponding to the two methods of analysis are shown in figure 8. Differences of 5 to 10% are obtained for the radiative heating-rate distributions, and convective heating-rate distributions differ by 10 to 15% in the region of laminar flow. In the turbulent flow region, the agreement between the two methods of analysis is unsatisfactory. The reason for the opposite trends in the turbulent heating-rate distributions corresponding to the two methods of analysis has not been determined. Additional calculations will be necessary to resolve these differences.

CONCLUDING REMARKS

The results of the present investigation demonstrate that numerically stable solutions to the viscous-shock-layer equations can be obtained for turbulent flows of radiating and nonradiating gas mixtures in chemical equilibrium. Acceptable agreement between the present method of analysis and an integral boundary-layer analysis is obtained for a nonradiating shock layer without injection of ablation products. The agreement between the present method of analysis and a solution which couples the inviscid flow and boundary-layer equations is unsatisfactory for the case of a radiating shock layer with ablation products injected into the layer. The limited availability of comparative data obtained with other methods of analysis is not sufficient to verify the present method of analysis.

REFERENCES

1. Sutton, Kenneth: Coupled Nongray Radiating Flow About Planetary Entry Bodies. AIAA J., Vol. 12, No. 8, Aug. 1974, pp. 1099-1105.

2. Moss, James N.: Stagnation and Downstream Viscous-Shock-Layer Solutions with Radiation and Coupled Ablation Injection. AIAA Paper No. 74-73, Jan. 1974.

3. Barnwell, R.W.: A Time-Dependent Method for Calculating Supersonic Angle-of-Attack Flow About Axisymmetric Blunt Bodies with Sharp Shoulders and Smooth Nonaxisymmetric Blunt Bodies. NASA TN D-6283, 1971.

4. Bartlett, E.P., and Kendall, R.M.: Nonsimilar Solution of the Multi-component Laminar Boundary Layer by an Integral Matrix Method. Aerotherm Corporation, Palo Alto, California, Aerotherm Report No. 66-7, Part III, March 14, 1967.

5. Davis, R.T.: Numerical Solution of the Hypersonic Viscous Shock-Layer Equations. AIAA J., Vol. 8, No. 5, May 1970, pp. 843-851.

6. Nicolet, W.E.: Advanced Methods for Calculating Radiation Transport in Ablation-Product Contaminated Boundary Layers. NASA CR-1656, 1970.

7. Nicolet, W.E.: User's Manual for the Generalized Radiation Transfer Code (RAD/EQUIL). NASA CR-116353, 1969.

8. Anderson, E.C., and Moss, J.N.: Numerical Solution of the Viscous-Shock-Layer Equations for Hypersonic Turbulent Flow of a Perfect Gas About Blunt Axially Symmetric Bodies. School of Engineering, Old Dominion University, Norfolk, VA, TR 74-T3, July 1974.

9. Bird, R.B., Stewart, W.E., and Lightfoot, E.N.: Transport phenomena. John Wiley & Sons, Inc., 1960.

10. Dorrance, William H.: Viscous Hypersonic Flow. McGraw-Hill Book Co., Inc., 1962.

11. Stroud, C.W., and Brinkley, Kay L.: Chemical Equilibrium of Ablation Materials Including Condensed Species. NASA TN D-5391, 1969.

12. Esch, D.D., Siripong, A., and Pike, R.W.: Thermodynamic Properties in Polynomial Form for Carbon, Hydrogen, Nitrogen, and Oxygen Systems from 300° to 15,000 °K. NASA CR-111989, 1970.

13. McBride, B.J., Heimel, S., Ehlers, J.G., and Gordon, S.: Thermodynamic Properties to 6000° K for 210 Substances Involving the First 18 Elements. NASA SP-3001, 1963.

14. Esch, D.D., Pike, R.W., Engel, C.D., Farmer, R.C., and Balhoff, J.F.: Stagnation Region Heating of a Phenolic-Nylon Ablator During Return From Planetary Missions. NASA CR-112026, 1971.

15. Wilke, C.R.: A Viscosity Equation for Gas Mixtures. J. Chem. Physics, Vol. 18, No. 4, April 1950, pp. 517-519.

16. Clauser, Francis H.: The Turbulent Boundary Layer. Vol. IV of Advances in Applied Mathematics, H.L. Dryden and Th. von Kármán, eds., Academic Press, Inc., 1956, pp. 1-51.

17. Klebanoff, P.S.: Characteristics of Turbulence in a Boundary Layer with Zero Pressure Gradient. NACA Rep. 1247, 1955. (Supersedes NACA TN 3178).

18. Cebeci, Tuncer: Behavior of Turbulent Flow Near a Porous Wall with Pressure Gradient. AIAA J., Vol. 8, No. 12, Dec. 1970, pp. 2152-2156.

19. Van Driest, E.R.: On Turbulent Flow Near a Wall. J. Aeronaut. Sci., Vol. 23, No. 11, Nov. 1956, pp. 1007-1011, 1036.

20. Edquist, C.T.: A Technique for Predicting Shock Induced Vorticity Effects During Venus Entry. R-70-48671-006, Martin Marietta Corp., Denver Division, Denver, Colorado, August 1970.

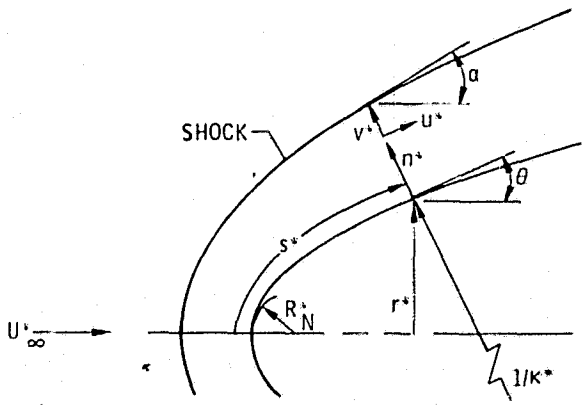

Figure 1. - Coordinate system.

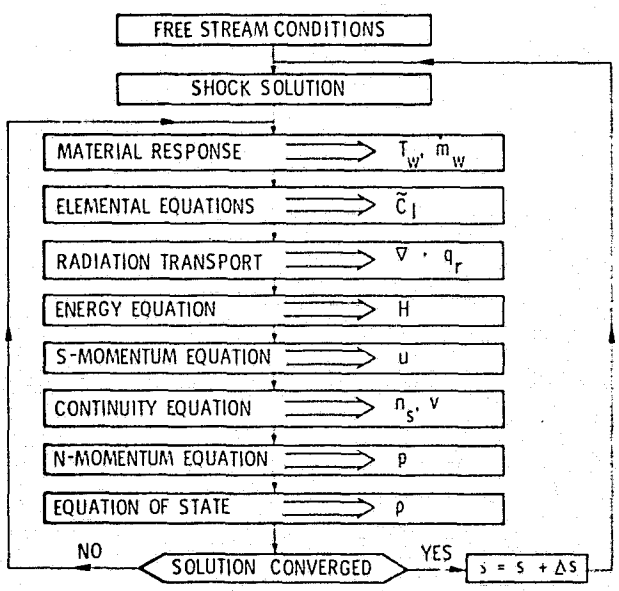

Figure 2. - Flow design of local solution procedure.

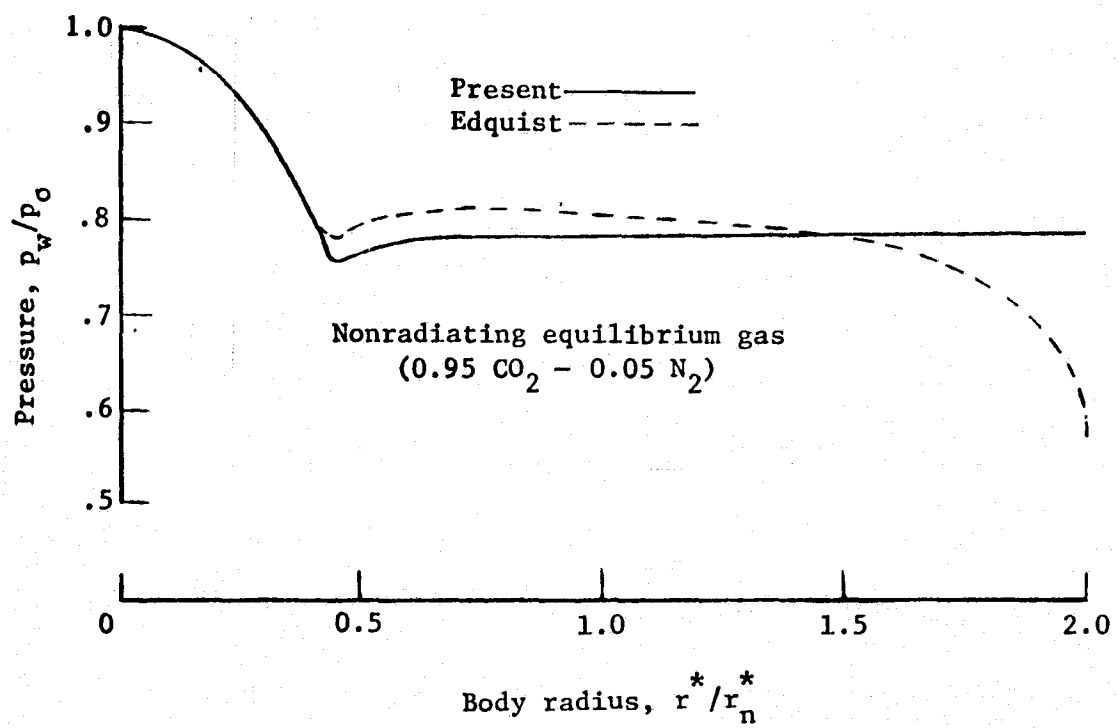

Figure 3. - Comparison of inviscid and viscous-shock-layer solutions for surface pressure distribution on a 120-degree sphere-cone.

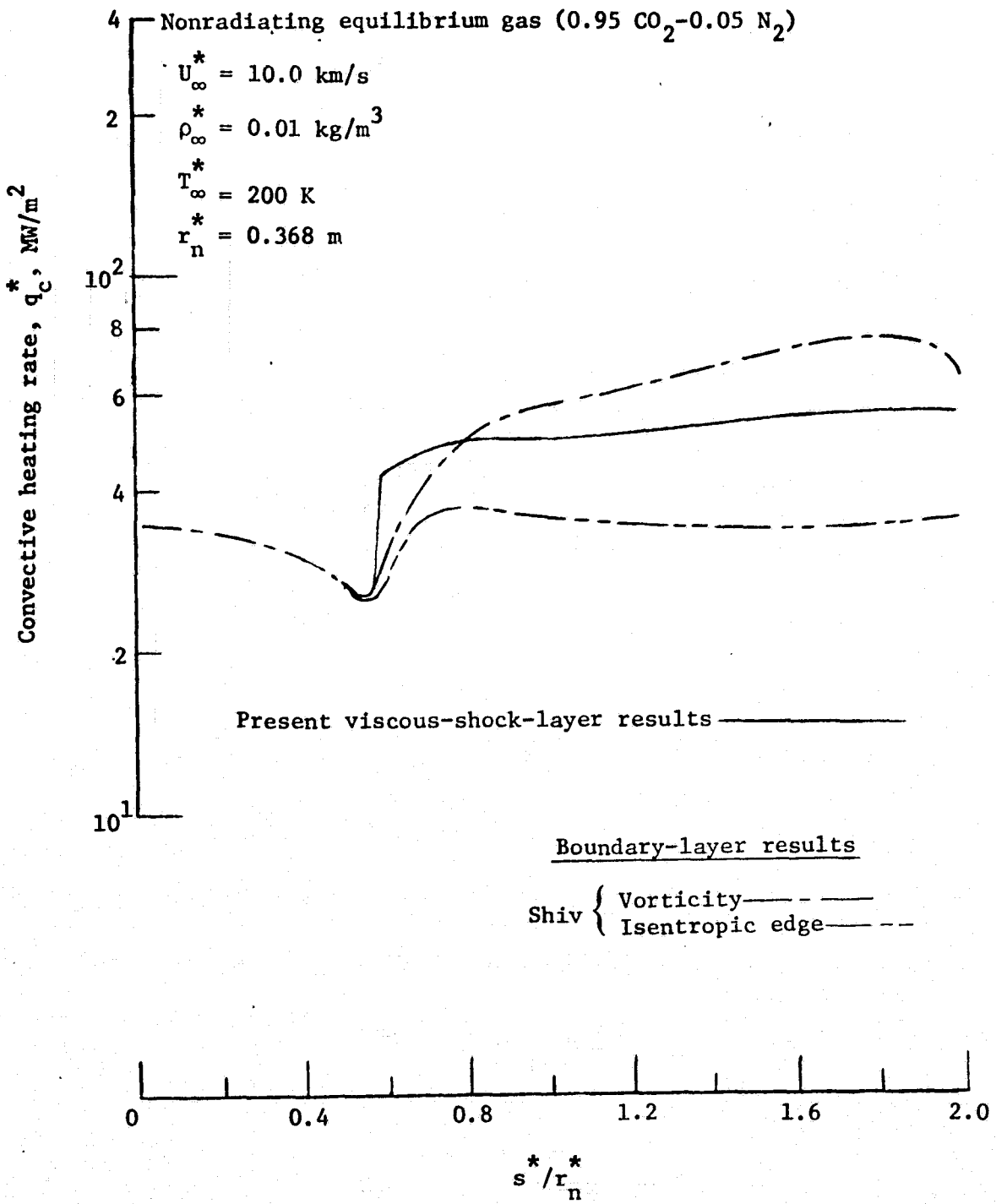

Figure 4. - Comparisons of heating-rate distribution on 120-degree sphere-cone.

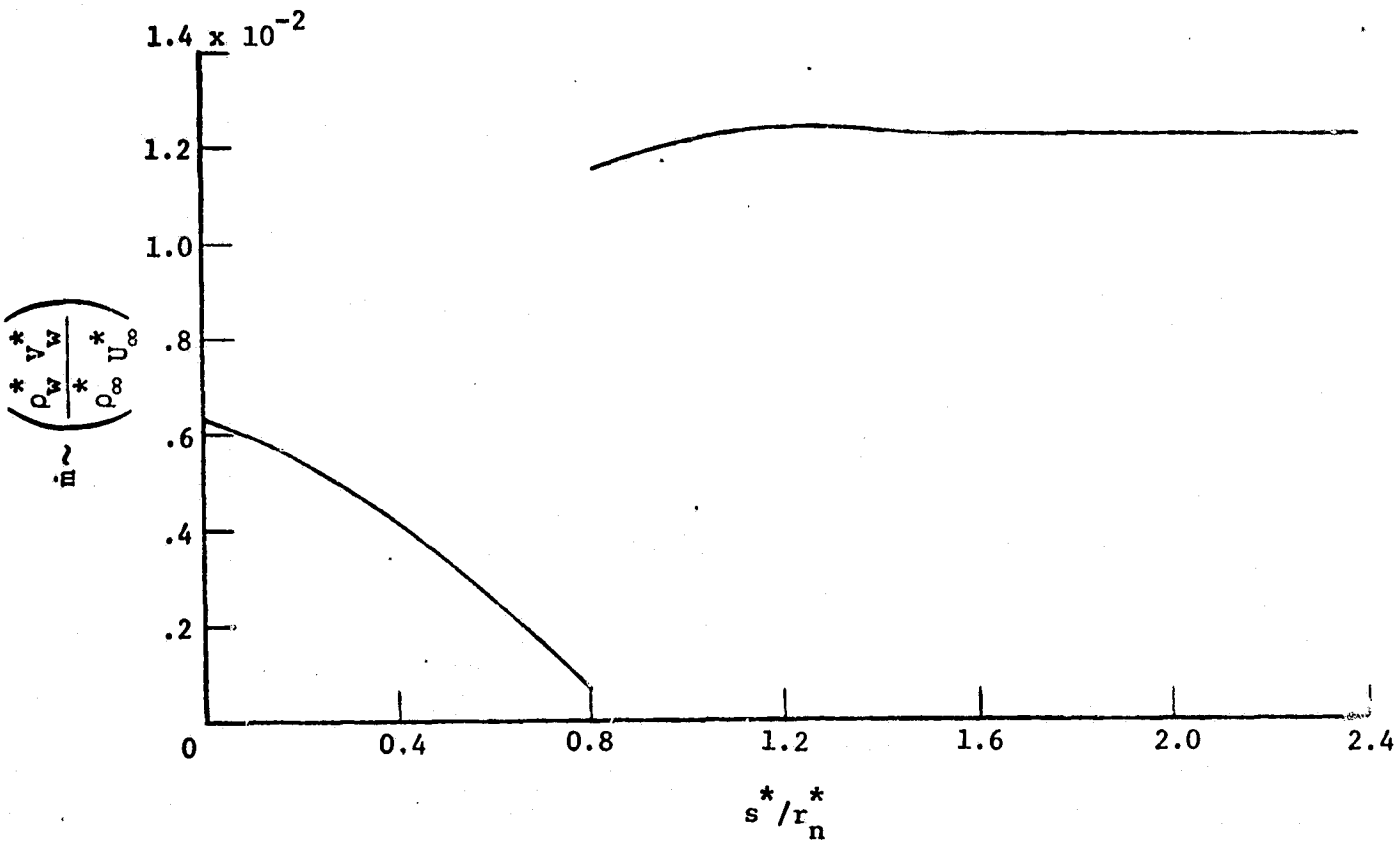

Figure 5. - Carbon-phenolic ablation-rate distribution for 120-degree sphere-cone.

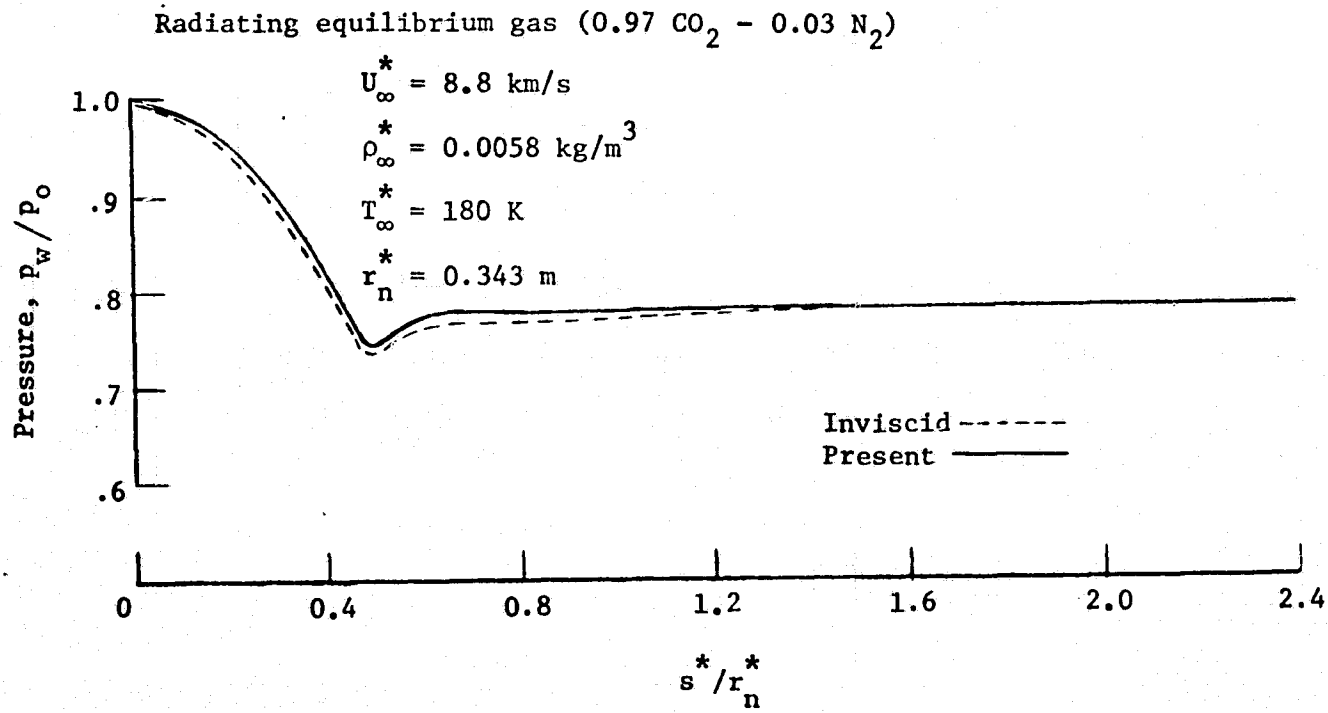

Figure 6. - Comparison of surface pressure distribution on 120-degree sphere-cone.

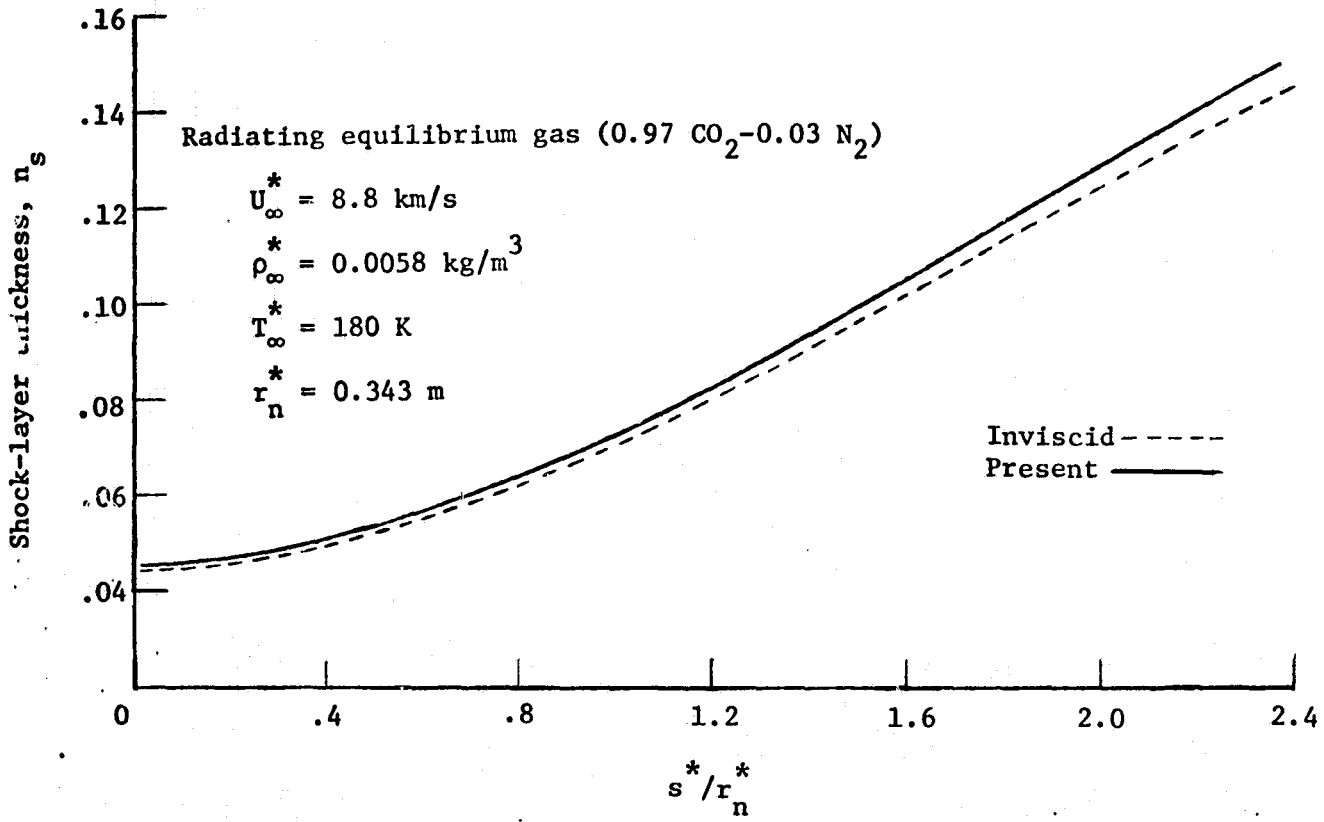

Figure 7. - Comparison of shock-layer thickness distribution.

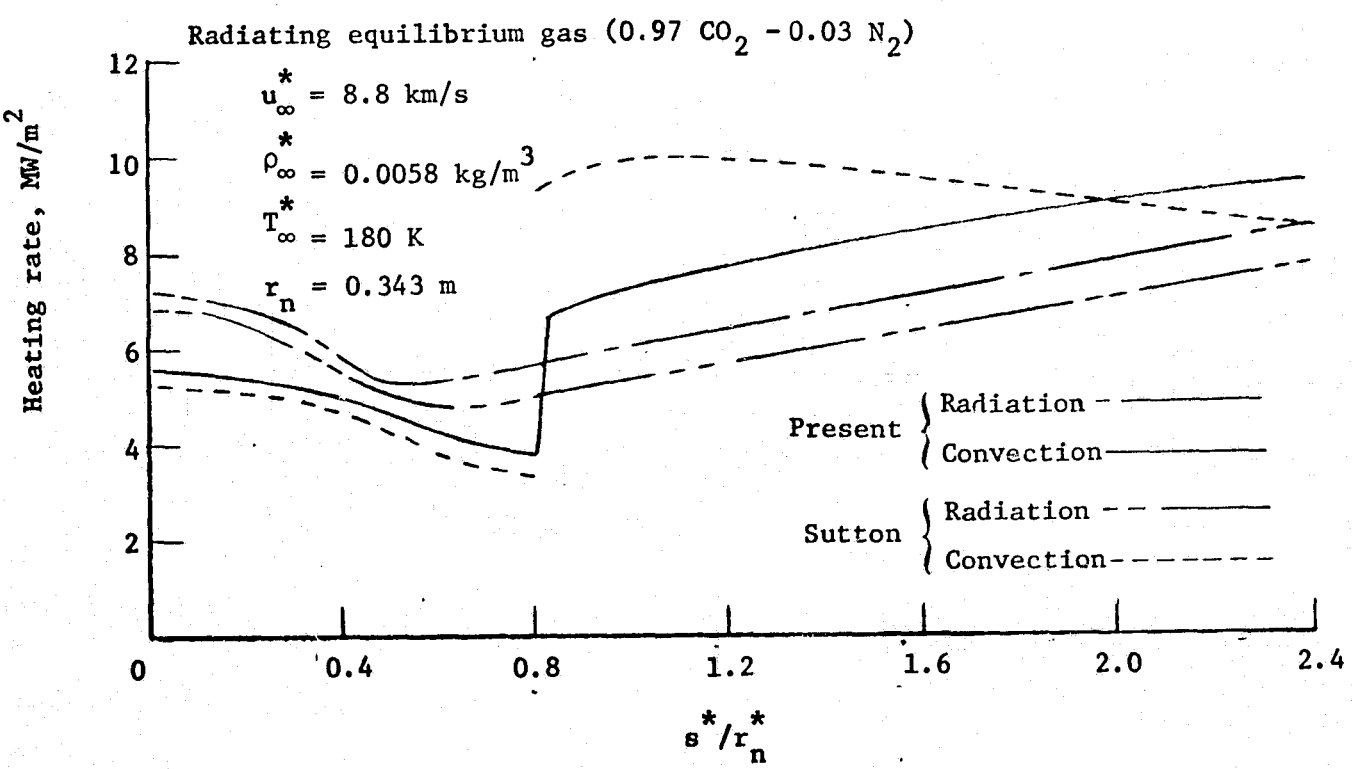

Figure 8. - Comparison of radiative and convective heating-rate distribution.